4. SUPERCONDUCTIVITY

(*) Not in Association framework

4. Super

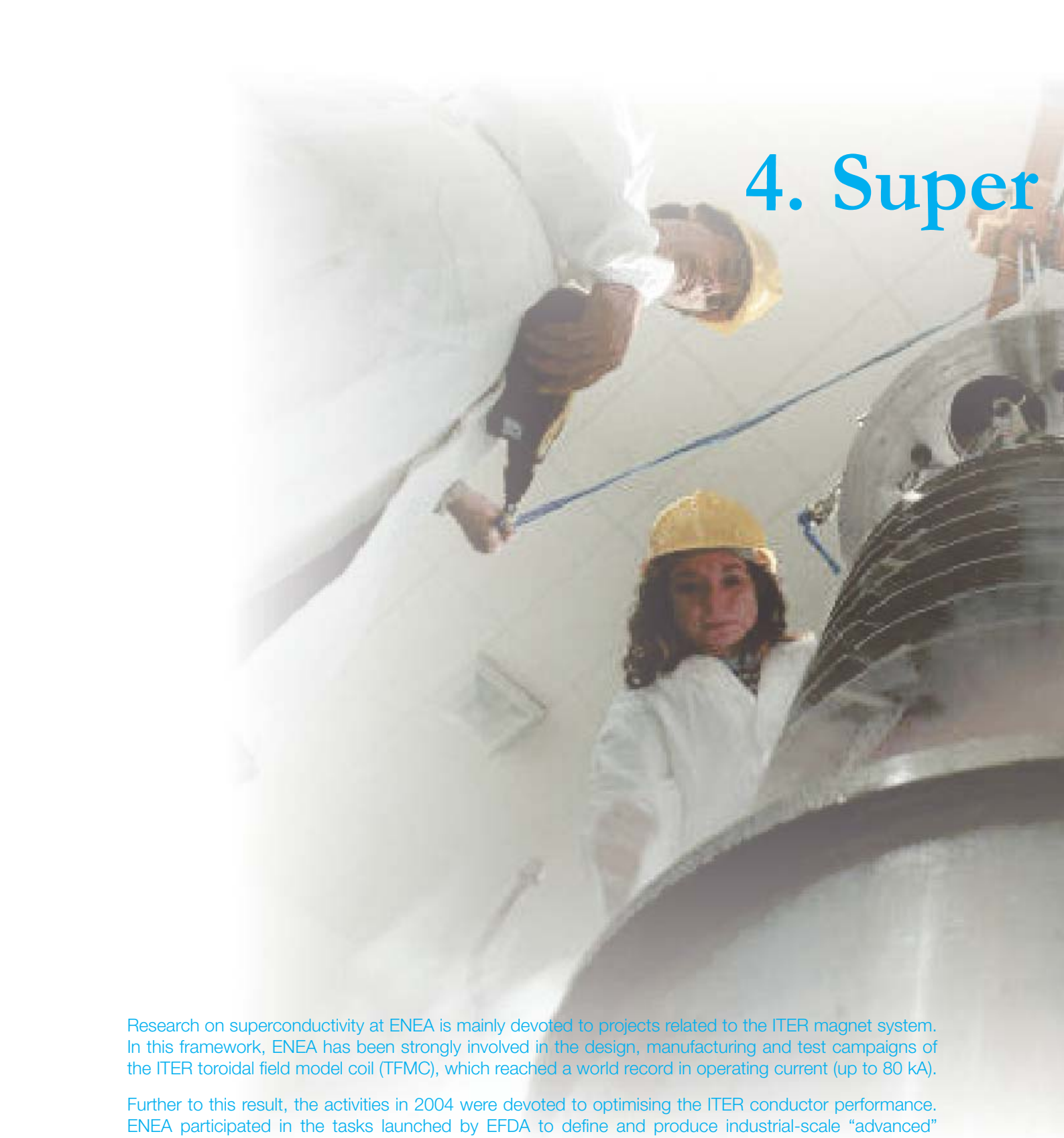

Research on superconductivity at ENEA is mainly devoted to projects related to the ITER magnet system. In this framework, ENEA has been strongly involved in the design, manufacturing and test campaigns of the ITER toroidal field model coil (TFMC), which reached a world record in operating current (up to 80 kA).

Further to this result, the activities in 2004 were devoted to optimising the ITER conductor performance. ENEA participated in the tasks launched by EFDA to define and produce industrial-scale “advanced” Nb_3Sn strand to be used in manufacturing the ITER high-field central solenoid (CS) and toroidal field (TF) magnets. As well as contributing to the design of the new strand and the final conductor layout, ENEA will also perform characterisation tests, addressing in particular the influence of mechanical stress on the Nb_3Sn performance. As a member of the international ITER-magnet testing group, ENEA plays a central role in the measurement campaigns and data analyses for each ITER-related conductor and coil. The next

conductivity

phase in the R&D of the ITER magnets will be their mechanical characterisation in order to define the fabrication route of the coils and structures.

During 2004 the cryogenic measurement campaign on the Large Hadron Collider (LHC) by-pass diode stacks was completed. As the diode-test activity was the only LHC contract to be finished on schedule, the Centre Europeènne pour la Recherché Nucléaire (CERN) asked ENEA to participate in an international tender for the cold check of the current leads for the LHC magnets. The contract was obtained, and during 2004, the experimental setup was designed and realised and the data acquisition system was developed. The measurement campaign was successfully started at the end of 2004 and will be completed in 2006.

4.2.1 Advanced Nb_3Sn strands

The new tasks on industrial-scale advanced Nb_3Sn strand also have the objective of stimulating the Nb_3Sn strand-production capabilities of European industries and encouraging them to reach the level achieved in Korea, the USA and Japan. An overall critical transport current of at least 200 A (at 12 T, 4.2 K, 0.1 μV/cm) will be required for the upgraded strand.

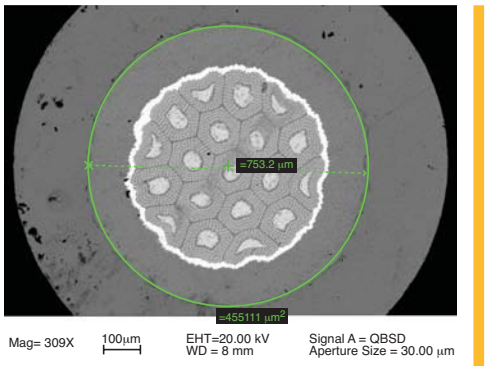

Fig. 4.1 - SEM micrograph of an internal tin advanced Nb_3Sn strand compacted inside a stainless steel jacket

A three-part programme has been set up under an ENEA-CEA Cadarache collaboration to experimentally assess the influence of mechanical stresses on the critical properties of the "new" Nb_3Sn strands inside stainless-steel-jacketed cable-in-conduit conductors (CICCs). It is well known that Nb_3Sn superconducting performance (i.e., J_C) strongly depends on applied mechanical stresses. In addition, on the scale of a single strand inside a CICC, the distributed bending strain could be responsible for the degradation in the performance of the cable compared to the virgin strand.

The first step will be an extended test of the performance of the advanced strands: strand layout, critical transport current, n-value, and room resistivity ratio will be measured, as well as hysteresis losses by a magnetisation technique [4.1].

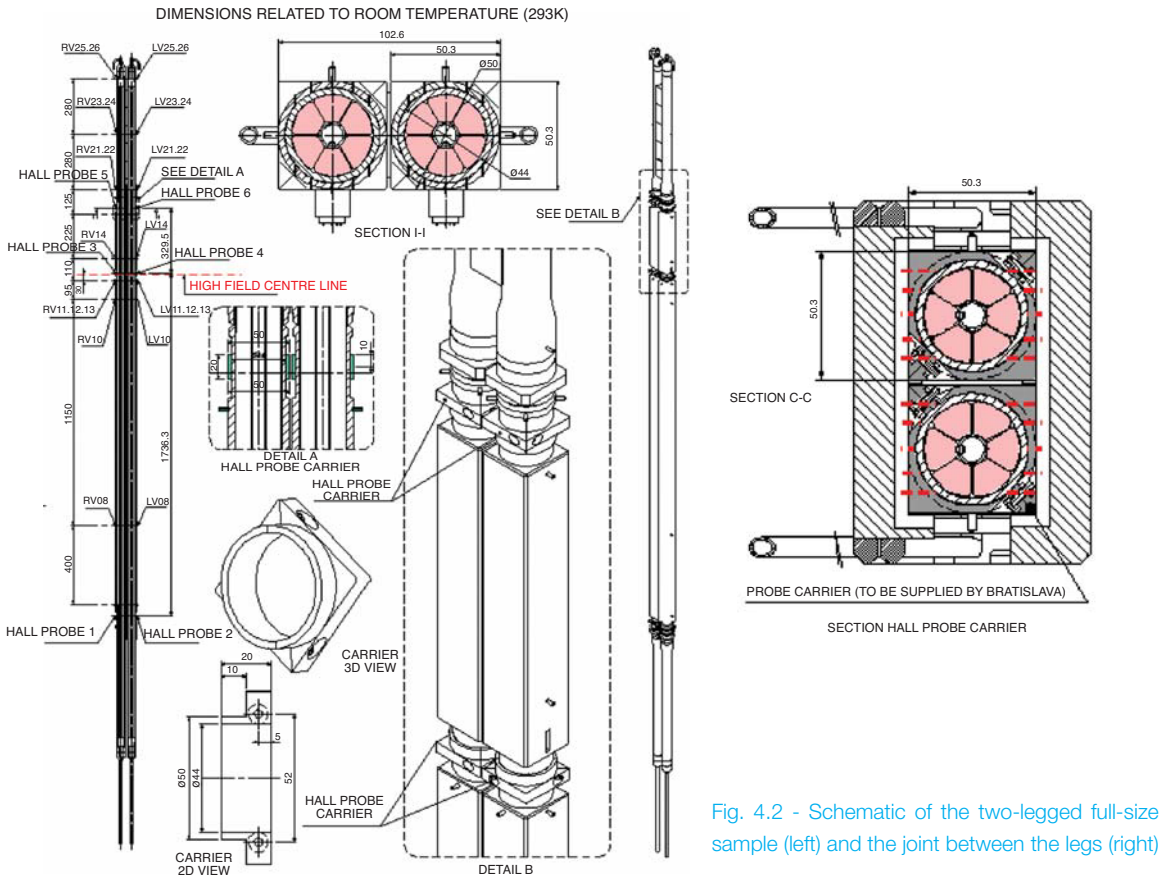

Fig. 4.2 - Schematic of the two-legged full-size sample (left) and the joint between the legs (right)

To investigate the bending strain effect, some strands will be heat-treated on barrel-type sample holders and then transferred onto different-diameter holders. The strands have been inserted and compacted inside a stainless steel jacket in order to impose a compressive longitudinal strain and provide strand support during sample handling procedures. The investigation will be extended in 2005 to sub-size cables (3/9/36/108 strands) as well as to ITER-type full-size cables made with the same advanced strands (fig. 4.1).

4.2.2 Participation in ITER testing campaigns: PF-FSJS tests at SULTAN

In spring 2004, the dc/ac performance of a two-legged straight poloidal field full-size joint sample (PF–FSJS) (fig. 4.2) was tested at the SULTAN facility of the Euratom-Swiss Confederation Association (CRPP) at Villigen. The two legs were manufactured with a NbTi full-size cable; one of the two legs has sub-cable wraps on the last-but-one cabling stage. The same conductor is being used for the manufacture of the poloidal field conductor insert, to be tested at Naka (Japan) under operating conditions relevant for the ITER PF1&6 coils.

ENEA was responsible for the conductor and SULTAN sample manufacture and also participated in the test campaign, data processing and analysis. The main results of the work were presented at the Symposium on Fusion Technology (SOFT) and the Applied Superconductivity Conference (ASC) in autumn 2004 [4.2-4.5].

4.2.3 Measurements on current distribution in cables: busbar III

It has been pointed out that one of the main issues influencing the performance of full-size ITER-relevant cables is the current distribution within the cable cross section: possible non-uniformities during both ramping and steady-state electromagnetic regimes may in fact cause degradation of the conductor performance (especially for NbTi cables), characterised by a limited temperature margin at operating conditions. Several experiments have therefore been devoted to investigating the mechanism of current distribution in full-size conductors. To measure the current flowing in each petal of the cable, it is necessary to adopt indirect current evaluation, that is, the magnetic field is measured in regions adjacent to the cable surface by means of Hall sensor heads placed around the conductor.

ENEA designed and realised the data acquisition systems for the Hall probe measuring heads and for all the sensors installed on the NbTi busbar III (BBIII), used as a short-circuit during the test of the high-temperature superconductor (HTS) current leads at FZK (figs. 4.3, 4.4). A part of the test campaign was devoted to current distribution measurements under different electromagnetic and thermo-hydraulic conditions. ENEA participated in the test campaign and collaborated in the data processing and analysis, with the aim of reconstructing the current distribution in the six petals of the conductor during operation. The main results were presented at the ASC in autumn 2004 [4.6].

References

[4.1] L. Muzzi, *Benchmarking and calibration tests of the testing facilities,* EFDA Task TW3-TMSC ASTEST, 1st Intermediate Report, 04/08/2004

[4.2] R. Wesche et al., *Analyses and implications of V-I characteristic of PF insert conductor sample*, presented at the 23rd Symp. on Fusion Technology - SOFT (Venice 2004)

[4.3] A. Formisano et al., *DC and transient current distribution analysis from self-field measurements on ITER PFIS conductor,* presented at the 23rd Symp. on Fusion Technology - SOFT (Venice 2004)

[4.4] P. Bruzzone et al., *Test results of the ITER PF insert conductor short sample in SULTAN,* presented at the Applied Superconducting Conference – ASC (Jacksonville 2004)

[4.5] Yu. A. Ilyin et al., *Effect of cycling loading and conductor layout on contact resistance of full-size ITER PFCI conductors*, presented at the Applied Superconducting Conference – ASC (Jacksonville 2004)

[4.6] R. Zanino et al., *Modeling AC losses in the ITER NbTi poloidal field full size joint sample (PF-FSJS) using the THELMA code*, to appear in Fusion Eng. Des.

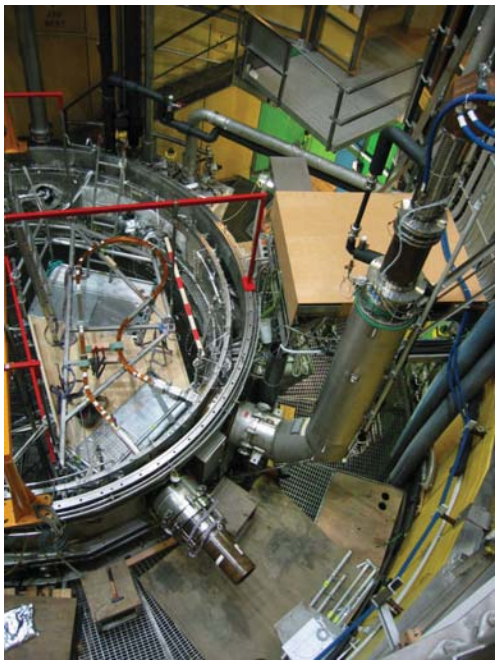

Fig. 4.3 - The curved BBIII short-circuiting the HTS current leads inside the TOSKA vessel (FZK)

Fig. 4.4 - The BBIII full-size conductor with the Hall probe circular heads for current distribution measurements

4.2.4 Code development and validation

The THELMA code is being developed by Turin Polytechnic (thermal-hydraulic module), the University of Bologna (electrical cable model) and the University of Udine (electrical joint model) in collaboration with ENEA and under the coordination of EFDA. The code is to be implemented in studies on coupled thermal-hydraulic electromagnetic transients in ITER CIC superconductors in order to compute (mainly) the current distribution on the conductor cross section, with particular emphasis on direct current performance (current sharing transition).

The code is being validated against alternating current loss data on the PF-FSJS [4.6,4.7]. In particular, it is being applied in the study of the so-called - and so far unexplained - premature quench in NbTi full-size CICC, as well as in the study of other dedicated experiments on NbTi. An effort to include an adequate mechanical description of the CICC is also in course with the University of Padua, with the objective of analysing Nb_3Sn strands and cables.

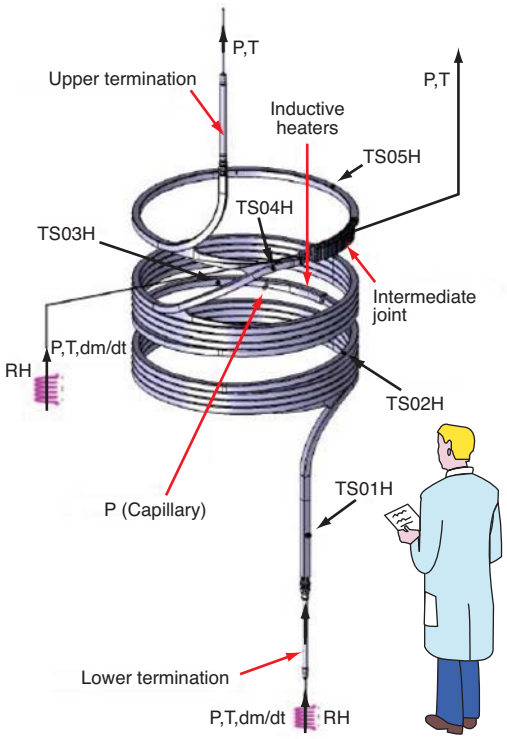

Fig. 4.5 - Sketch of the ITER poloidal field coil insert. Main winding (lower) and NbTi busbar (upper) are electrically connected by the intermediate joint and separately cooled by independent helium circuits

4.2.5 Poloidal field coil insert

To date, the behaviour of ITER-type NbTi CICC has mainly been assessed on the basis of extended characterisation of sub-size samples, short full-size samples and joints [4.8,4.9]. The results of these tests indicate that some issues need deeper analysis. For example, the so-called "sudden quench" phenomenon (i.e., when the cable reaches critical conditions at currents and/or temperatures lower than what is expected from single-strand performance and, indeed, below the ITER requirements) requires further investigations to be made on longer lengths of coiled full-size conductor. To this end, the ITER poloidal field conductor designed by ENEA, manufactured by Ansaldo Superconduttori and used for the coil winding at Tesla Engineering, UK in the framework of a Task Agreement with the ITER International Team, will be tested at JAERI [4.10].

The conductor is NbTi dual-channel, about 45m long, with a 50-mm-thick square stainless steel jacket, wound in a single-layer solenoid (fig. 4.5). It should carry up to 50 kA in a field of ~6 T and will be cooled by supercritical He at ~4.5 K and ~0.6 MPa. An intermediate connection, representative of the ITER poloidal field joints [4.11] and located at relatively high field, will be an important new item in the test configuration with respect to the previous ITER insert coils.

The main winding and the upper busbar have been completed. The coil should be impregnated by September 2005 and assembled and shipped to the Naka facility by November 2005. The test programme will include dc and pulsed performance assessment of the conductor and the intermediate joint, ac loss measurement, stability, quench propagation and thermo-hydraulic characterisation. ENEA is one of the principal operators in the project and, in particular, has been entrusted with designing the data acquisition system for the current distribution measurements, given the high-quality performance of an analogous system developed by ENEA for similar measurements carried out on the TFMC busbar during the phase-II test campaign at FZK, the HTc current lead short circuit (Busbar III), again at FZK, and on the poloidal field insert sample at SULTAN.

4.3 Advanced Stability Experiment (ASTEX)

The current inside multifilamentary/multistage conductors can be distributed nonuniformly among different strands or cable sub-elements both during steady-state operation, owing to the different contact resistance of each cable element at the joint, and during current variations, because of the different effective inductance of each sub-element. This has been identified as the main cause of premature conductor quench phenomena or current ramp-rate limitations.

ENEA has planned an experiment, currently in its installation phase, to study the influence of current distribution on conductor properties, such as critical current, ac losses and stability [4.12]. A magnet has been coil wound with a subsize

References

[4.7] M. Ciotti et al., *Validation of the THELMA code against data from the ENEA stability experiment database,* submitted to Cryogenics

[4.8] P. Bruzzone et al., *Test results of the ITER PF insert conductor short sample in SULTAN,* presented at the Applied Superconducting Conference – ASC (Jacksonville 2004)

[4.9] R. Zanino et al., *Current distribution measurement on the ITER-type NbTi Bus Bar III*, presented at the Applied Superconducting Conference – ASC (Jacksonville 2004)

[4.10] R. Zanino et al., *Preparation of the ITER poloidal field conductor insert (PFCI) test*, presented at the Applied Superconducting Conference – ASC, (Jacksonville 2004)

[4.11] F. Hurd, et al., *Design and manufacture of a full size joint sample (FSJS) for the qualification of the poloidal field (PF) insert coil,* presented at the Applied Superconducting Conference – ASC (Jacksonville 2004)

[4.12] A. della Corte et al., *Design and manufacture of a NbTi insert module relevant for the ITER PF magnets conductor*, presented at the Inter. Cryogenic Engineering Conference - ICEC-20 (Beijing 2004)

NbTi 36-strand conductor opened at both terminations and subdivided into four 9-strand last-but-one stages, one of which further subdivided in two parts: triplet and the remaining 6 strands. These sub-stages will be connected to the power supply by means of the same type of HTc leads (fig. 4.6) as designed for the LHC and under testing at ENEA: this will be the last upgrade to the ASTEX facility. A system of external resistors allows the magnet to be supplied with a controlled nonuniformly distributed current. The module is fully instrumented with thermometers, voltage taps, pickup coils, pressure gauges and helium mass flow meters for characterising its behaviour during both steady-state operation and current variations.

The experimental campaign will start in the first months of 2005.

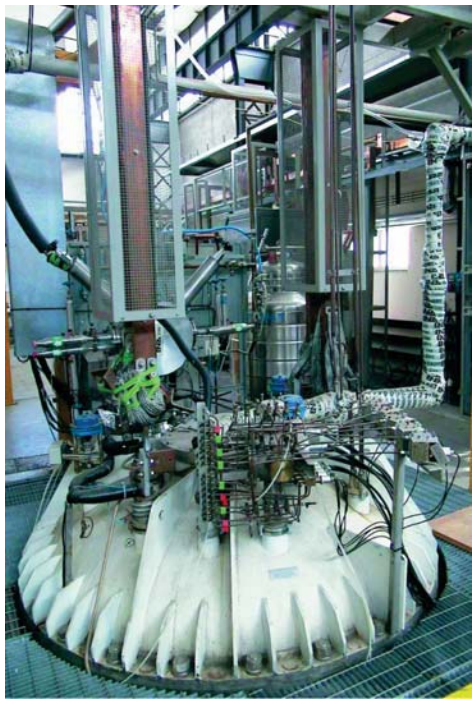

Fig. 4.6 - ENEA facility for testing superconducting solenoid magnets

4.4.1 Cryogenic testing of diode stacks

Testing of the by-pass diodes for quench protection of the dipole and quadrupole magnets of the LHC at CERN was completed on schedule thereby guaranteeing completion of the measurement campaign on all the stacks (1250 for the dipoles, 400 for the quadrupoles) within 2004 [4.13]. As agreed with CERN, a few diode stacks whose performance was uncertain during the first characterisation measurements will be re-tested at ENEA in early 2005.

By this contract ENEA was paid about 1.2 M€ including in-kind contributions.

Fig. 4.7 - Connection between CERN 13-kA HTS leads and the bars of the ENEA power supply devoted to the test

4.4.2 Cryogenic testing of current leads

The LHC will have about 8000 superconducting magnets with different current ratings. To power the magnets, more than 1000 HTS leads installed inside the liquid helium vessel will be needed to provide the electrical connection between the warm cables to/from the power converter and low-temperature superconducting busbar carrying the current to/from the cryomagnets. Therefore, the leads will have to operate in a temperature range between room and liquid helium.

ENEA has been contracted by CERN to perform the cold check of the leads, simulating the operating conditions. The experimental setup has been designed and constructed according to the typical criterion of a scientific experiment, but the test site has been dimensioned to meet the schedule of an industrial-scale activity, due to the huge quantity of devices to be tested. ENEA has also developed a dedicated data acquisition system (fig. 4.7).

The measurement campaign started at the end of 2004 and the testing results completely fulfilled CERN requirements.

4.5.1 Development of metallic coated substrate for HTS tapes

Silver is the most widely employed material for BSCCO wires and tapes because of its chemical inertia with the superconductor as well as with its precursors. However, a pure Ag substrate has two major drawbacks - high cost and poor mechanical properties at high temperatures. To improve the physical properties of the substrate, without loosing the chemical properties, Ag-buffered Ni-based tapes have been studied [4.14–4.15].

As reported in [4.15-4.17], dewetting of the Ag film occurs during annealing in air, and pin holes appear on its surface. These holes cause chemical contamination from the substrate to the superconductor with infiltration of liquid phases during high-temperature Bi-2212 synthesis, which can suppress the superconductivity. The introduction of a buffer layer between Ag and Ni tape could be a suitable way to reduce the dewetting mechanism and avoid Bi-2212 contamination by Ni.

EDISON S.p.A. and ENEA collaborated during 2002-2004 with the aim of optimising such a buffer layer. Controlled oxidation of the substrate and deposition of ceramic film (MgO, CeO_2,YSZ,...) between NiCr tape and silver film via e-beam evaporation were investigated.
To verify the chemical composition, morphology and effective barrier efficiency, extended characterisation of the buffered substrate was performed by scanning electron microscopy (SEM), electron backscattering diffraction (EBSD) and x-ray diffraction (XRD) analyses, also after thermal treatment of the samples at 850°C in oxygen. Among the various choices, CeO_2 exhibits the best buffer-layer performance, with no Ag film dewetting or degradation, but it suffers from mechanical stress at high temperatures.

It is supposed that Ag film instabilities are mainly due to the high interface energy between the metallic and the oxide films. As it is well known that a binary alloy has a lower Gibbs free energy than pure metals, a thin Pd film was interposed between the above mentioned CeO_2 buffer layer and the Ag film. Pd was chosen because it forms a complete solid solution with Ag at all the relative concentrations. This approach permits complete inhibition of hole formation.

4.5.2 Development of (YBCO) based coated conductor tapes

The activities were focussed on developing $YBa_2Cu_3O_{7-x}$ (YBCO) based coated conductor tapes, mainly by improving the electrical transport properties and developing chemical solution deposition methods for epitaxial YBCO films.

Two different substrates were taken into account: $Ni_{95}W_5$ (Ni–W) and $Ni_{88}Cr_8W_4$ (Ni-Cr-W) [4.18,4.19]. It was demonstrated that an intermediate layer of Pd between the substrate and the oxide buffer layer architecture can reduce contamination from the substrate and improve the structural and - consequently – the superconducting properties of YBCO film [4.19,4.20]. The effect of partial substitution of Y with Ca on the transport properties of YBCO thin film [4.21,4.22] was also investigated.

References

[4.13] A. Gharib et al. Adv. Cryog. Eng. **50**, 755-762 (2004)

[4.14] P. Régnier et al., Physica C **372-376**, 923-926 (2002)

[4.15] P. Régnier et al., Superc. Sci. Technol. **15**, 1427-1435 (2002)

[4.16] L. Schirmgeld-Mignot et al., Phil. Mag. Lett. **80**, 33-40 (2000)

[4.17] H. De Monestrol et al., Acta Mater. **49**, 1655-1660 (2001)

[4.18] A. Vannozzi et al., *Texture evolution and stability of Ni-W substrates for YBCO coated contuctors*, presented at Spectroscopy on Novel Superconductors SNS'2004 Conference (Sitges 2004)

[4.19] G. Celentano et al., *YBCO films and CeO_2/YSZ/CeO_2 buffer layers grown on Ni-Cr-W RABiTS with a Pd seed layer,* to appear in IEEE Trans. Appl. Supercond.

[4.20] A. Mancini et al., *Microstructural study of $YBa_2Cu_3O_{7-x}$ thin films prepared by TFA-MOD method,* presented at the Applied Superconducting Conference – ASC (Jacksonville 2004)

[4.21] A. Augieri et al., Physica **C401**, 320 (2004)

[4.22] C. Cancellieri et al.,*Deposition and characterization of $Y_{1-x}CaxBa_2Cu_3O_{7-x}$ epitaxial thin films,* to appear in IEEE Trans. Appl. Supercond.

Chemical-solution deposition methods for epitaxial thin-film fabrication are of scientific interest in the development of superconducting materials because of their relative simplicity and precise stoichiometric control. Among the different techniques, it has been demonstrated that the trifluoroacetate metal-organic decomposition (TFA-MOD) method is the most suitable for low-cost epitaxial YBCO deposition.

Texture and microstructure stability of Ni-W metallic substrate. To develop a suitable texture for YBCO epitaxial growth, the metallic substrates were thermo-mechanically treated. Then, to ensure stable texture and microstructure under film growth conditions, the structural and morphological evolution of Ni–W substrate subjected to thermal treatments was studied [4.18]. Tapes were annealed in high vacuum at different temperatures ranging from 400 to 1000°C, and for times ranging from 0 to 4 h. The deformation texture, mainly β fibre, was not affected by annealing up to 600°C; between 700 and 800°C, cube texture and deformation texture coexisted and at higher temperatures the sample was only cube textured. These features are reported in figure 4.8, which shows the φ-scans at χ=54.7° for the (111) Ni-W peak; the evolution of cube texture is related to the increase of the peak at φ=45°. To evaluate the microstructural stability, EBSD analyses were performed for samples recrystallised at 940°C for different times before and after a successive annealing to simulate YBCO film deposition (850°C for 30 min). For recrystallisation times shorter than 20 min (fig. 4.9), the microstructure was unstable and grain boundary migration was observed, particularly between highly misoriented grains, such as the cubic twin of the {221}<122> grain that grows during the thermal treatment.

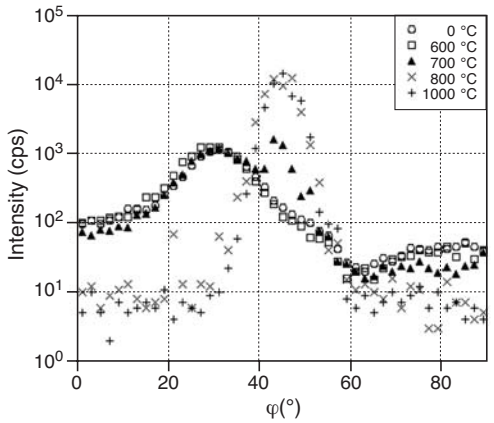

Fig. 4.8 - φ-scans at χ=54.7° for (111) Ni-W peak for samples annealed at different temperatures

Ni-Cr-W substrate with Pd intermediate layer. It has already been observed that YBCO film deposited on Ni-Cr-W substrate is affected by local Ni poisoning and structural disorder in grooved grain boundaries. To enhance the YBCO film properties, a Pd intermediate layer was deposited between substrate and CeO_2/YSZ/CeO_2 buffer layer architecture by electron beam evaporation at a substrate temperature of 400°C [4.19]. Then the sample was moved into a vacuum chamber equipped for pulsed laser deposition (PLD) of oxides and YBCO. The CeO_2/YSZ buffer layers were deposited at low temperature (500°C) in order to limit the Pd-substrate interdiffusion effect. CeO_2 cap layer and YBCO were deposited at 850°C. Despite Pd-substrate interdiffusion at high temperature, good structural and morphological properties both for the buffer layers and for the YBCO film were obtained (figs. 4.10 and 4.11). T_c of about 89 K and I_c=3.1 A in self-field and 77 K were measured, for a resulting J_c of about 0.4 MA/cm^2 (figs. 4.12 and 4.13). These improved electrical properties, compared to those previously reported for this substrate, suggest that a Pd layer may reduce contamination of the YBCO film.

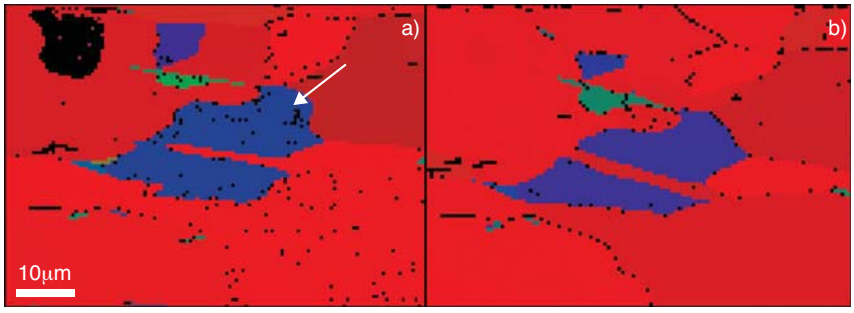

Fig. 4.9 - EBSD maps with respect to the normal direction of a Ni-W sample recrystallised at 940°C for 5 min before a) and after b) simulation treatment at 850°C for 30 min. Red, green and blue refer to {001}, {011} and {111} orientations, respectively. Arrow marks the cubic twin of the {221}<122> grain

YBCO thin films prepared by TFA-MOD method. The TFA-MOD process was used to grow YBCO films with a

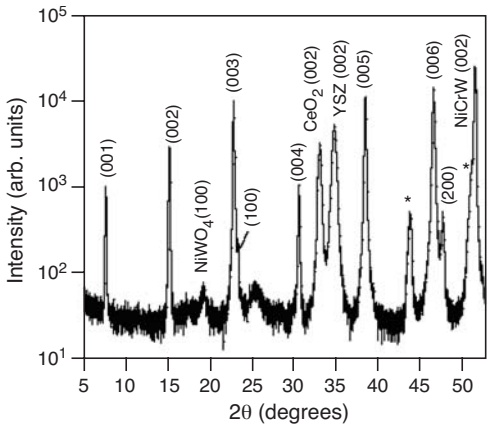

Fig. 4.10 - θ-2θ x-ray diffraction pattern of YBCO/CeO_2/YSZ/CeO_2/Pd architecture grown on Ni-Cr-W substrate. Star marks peaks related to Pd-Ni solid solution

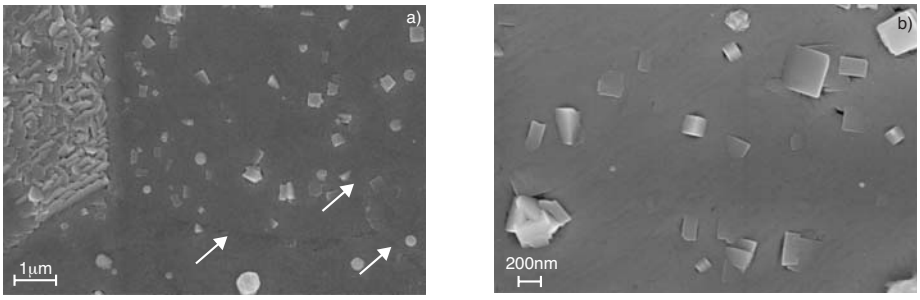

Fig. 4.11 - a) SEM image of YBCO film surface. Top left corner: YBCO grown on a misoriented substrate grain. White arrows: substrate low-angle grain boundaries. b) (00l) YBCO surface at higher magnification showing outgrowths, holes and droplets typical of PLD deposition

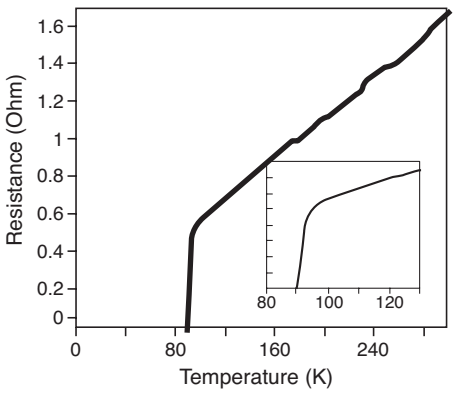

Fig. 4.12 - Temperature dependence of electrical resistance for YBCO film deposited on CeO_2/YSZ/ CeO_2/Pd buffered Ni-Cr-W substrate. Insert: detail of the transition region

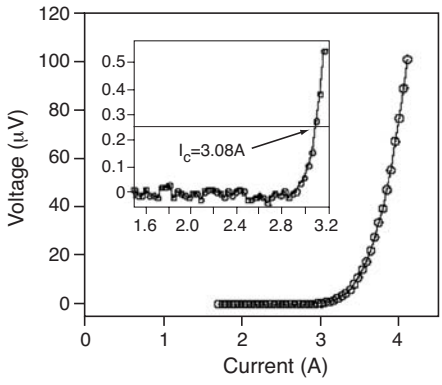

Fig. 4.13 - I-V characteristic for a 2.6-mm-wide YBCO strip deposited on Ni-Cr-W/Pd/CeO_2/YSZ/CeO_2 recorded at 77 K and self-field. Insert: transition region magnified; the I_c value is determined by the 1 μV/cm criterion

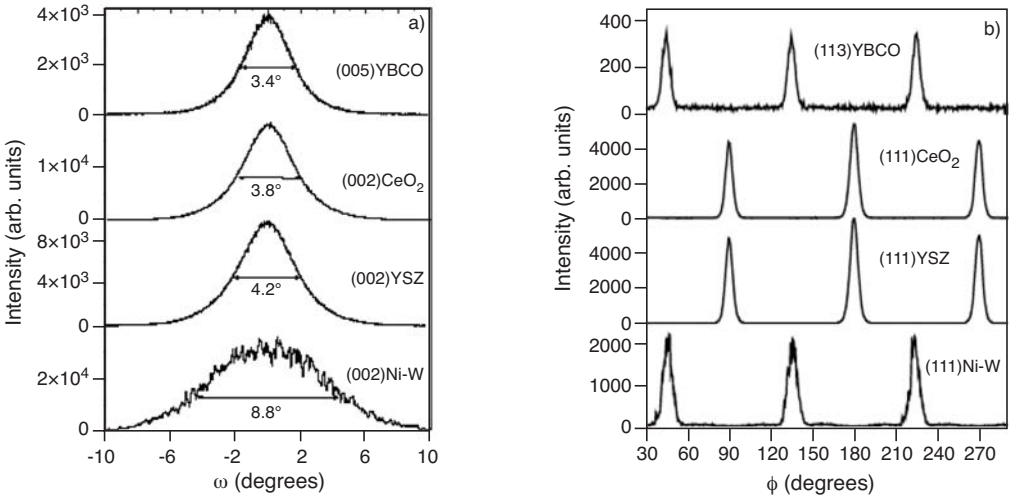

Fig. 4.14 - a) ω -scan of the (002)Ni-W, (002)YSZ, (002)CeO_2 and (005)YBCO peaks. b) ϕ -scans of (113)YBCO, (111)CeO_2, (111)YSZ and (111)Ni-W peaks

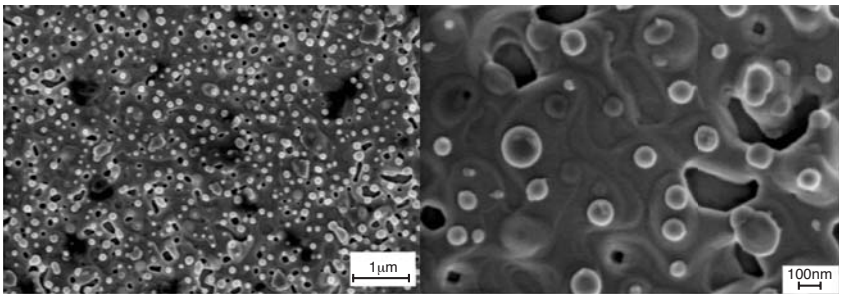

Fig. 4.15 - SEM image of YBCO/ CeO_2/YSZ/CeO_2/Pd/Ni-W film surface

high degree of epitaxy both on (100)$SrTiO_3$ single crystal and on Pd/CeO_2/YSZ/CeO_2 buffered Ni-W [4.20]. The x–ray study revealed that the Pd film has a better in-plane and out-of-plane texture than the Ni-W substrates (fig. 4.14). This explains the excellent structural properties of YBCO film grown on the as-buffered substrate. The SEM investigation revealed that the YBCO film on Ni-W has a good surface with well connected c-axis oriented grains that suggests good transport properties (fig. 4.15). This study has demonstrated that the CeO_2/YSZ/CeO_2/Pd buffer layer architecture is adequate for manufacturing long YBCO tapes on Ni-W substrates. Future activity will be focussed on the preparation and electrical characterisation of long YBCO superconducting tapes.

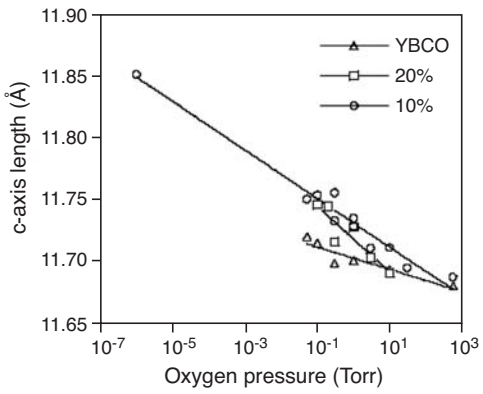

Fig. 4.16 - c-axis vs. annealing oxygen pressure for all three Ca concentrations

Effect of Ca substitution in YBCO thin films. Samples of Ca-substituted YBCO thin films were deposited by laser ablation on $SrTiO_3$ single-crystal substrates, varying the Ca amount by 0, 10 and 20 atomic percent, i.e., $Y_{1-y}Ca_xBa_2Cu_3O_{7-x}$ with y=0, 0.1, 0.2. Since the annealing

treatment affects the oxygen content of the films, it was varied by thermal treatment under different oxygen pressures and its effects on the electrical and structural properties were investigated. The c-axis of Ca-substituted YBCO decreases from 11.85 to 11.68 Å with increasing annealing oxygen pressure (fig. 4.16). The critical temperature was optimised for all three Ca concentrations studied at a fixed annealing time of 1 h. The T_c dependence on annealing oxygen pressure reveals the presence of an overdoping region in the charge carrier concentration in Ca-substituted films (fig. 4.17). This region is remarkably reduced when extending the annealing time to several hours. These data suggest the presence of an overdoping region in Ca-YBCO, which is reduced when the annealing time is extended to several hours. This implies that the maximum overdoping level is uncertain due to the superposition of cation disorder effects on T_c values.

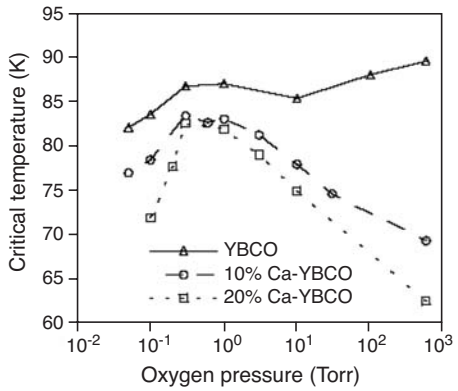

Fig. 4.17 - T_c vs. annealing pressure for all three Ca concentrations. Annealing time was 1 h.